nanomaterials

MDPI

Review

Novel Architecture Titanium Carbide ($Ti_3C_2T_x$) MXene Cocatalysts toward Photocatalytic Hydrogen Production: A Mini-Review

Van-Huy Nguyen [1,2,*], Ba-Son Nguyen [3], Chechia Hu [4], Chinh Chien Nguyen [5,6], Dang Le Tri Nguyen [5], Minh Tuan Nguyen Dinh [7], Dai-Viet N. Vo [8], Quang Thang Trinh [9], Mohammadreza Shokouhimehr [10], Amirhossein Hasani [11], Soo Young Kim [12,*] and Quyet Van Le [5,*]

1 Department for Management of Science and Technology Development, Ton Duc Thang University, Ho Chi Minh City 700000, Vietnam
2 Faculty of Applied Sciences, Ton Duc Thang University, Ho Chi Minh City 700000, Vietnam
3 Key Laboratory of Advanced Materials for Energy and Environmental Applications, Lac Hong University, Bien Hoa 810000, Vietnam; nbsonhd@gmail.com
4 Department of Chemical Engineering, R&D center for Membrane Technology and Research Center for Circular Economy, Chung Yuan Christian University, Chungli Dist., Taoyuan City 32023, Taiwan; chechiahu@cycu.edu.tw
5 Institute of Research and Development, Duy Tan University, Danang 550000, Vietnam; nguyenchinhchien@duytan.edu.vn (C.C.N.); dltnguyen@yahoo.com (D.L.T.N.)
6 Faculty of Environmental and Chemical Engineering, Duy Tan University, Da Nang 550000, Vietnam
7 Faculty of Chemical Engineering, University of Science and Technology, The University of Da Nang, 54 Nguyen Luong Bang, Da Nang 550000, Vietnam; ndmtuan@dut.udn.vn
8 Center of Excellence for Green Energy and Environmental Nanomaterials (CE@GrEEN), Nguyen Tat Thanh University, 300A Nguyen Tat Thanh, District 4, Ho Chi Minh City 755414, Vietnam; daivietvnn@yahoo.com
9 Cambridge Centre for Advanced Research and Education in Singapore (CARES), Campus for Research Excellence and Technological Enterprise (CREATE), 1 Create Way, Singapore 138602, Singapore; qttrinh@ntu.edu.sg
10 Department of Materials Science and Engineering, Research Institute of Advanced Materials, Seoul National University, Seoul 08826, Korea; mrsh2@snu.ac.kr
11 School of Chemical Engineering and Materials Science, Chung-Ang University, Seoul 06974, Korea; amirhossein.hasani88@gmail.com
12 Department of Materials Science and Engineering, Korea University, 145 Anam-ro, Seongbuk-gu, Seoul 02841, Korea
* Correspondence: nguyenvanhuy@tdtu.edu.vn (V.-H.N); sooyoungkim@korea.ac.kr (S.Y.K.); levanquyet@dtu.edu.vn (Q.V.L.); Tel.: +84-968-485-175 (V.-H.N.); +82-109-3650-910 (S.Y.K.); +84-344-176-848 (Q.V.L.)

Received: 26 February 2020; Accepted: 23 March 2020; Published: 25 March 2020

Abstract: Low dimensional transition metal carbide and nitride (MXenes) have been emerging as frontier materials for energy storage and conversion. $Ti_3C_2T_x$ was the first MXenes that discovered and soon become the most widely investigated among the MXenes family. Interestingly, $Ti_3C_2T_x$ exhibits ultrahigh catalytic activity towards the hydrogen evolution reaction. In addition, $Ti_3C_2T_x$ is electronically conductive, and its optical bandgap is tunable in the visible region, making it become one of the most promising candidates for the photocatalytic hydrogen evolution reaction (HER). In this review, we provide comprehensive strategies for the utilization of $Ti_3C_2T_x$ as a catalyst for improving solar-driven HER, including surface functional groups engineering, structural modification, and cocatalyst coupling. In addition, the reaming obstacle for using these materials in a practical system is evaluated. Finally, the direction for the future development of these materials featuring high photocatalytic activity toward HER is discussed.

Keywords: photocatalysis; $Ti_3C_2T_x$; MXenes; photocatalysis; water splitting; HER

1. Introduction

To date, sustainable solar hydrogen (H_2) production, which directly produces by utilizing semiconductor photocatalysts, could provide a promising and environmental-friendly approach to solve the worldwide energy issues and reduce the dependence on fossil fuels [1,2]. Particularly, enormous progress has been made in developing a new system of photocatalysts such as transition metal dichalcogenides [3–15], transition metal oxide (TMOs) [16,17], transient metal sulfides (TMSs), graphitic carbon nitride (*g*–C_3N_4) [18–22], metal–organic framework (MOFs) [23–25], transition metal nitride (TMNs) [26], and transition metal carbide (TMCs) [27–30] that could efficiently enhance the H_2 production, and readily scale up for commercialization [2].

As an advanced and broad group of novel nanostructured materials, MXenes has been discovered and synthesized from the parent layered solids MAX phases (as shown in Figure 1) [31].

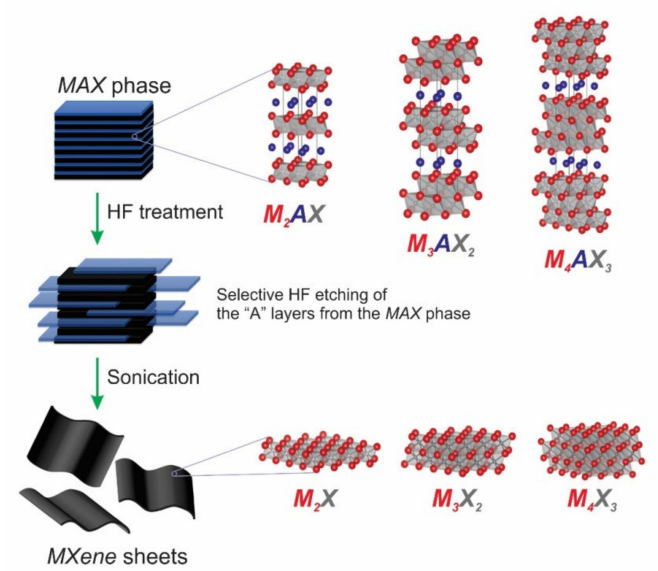

Figure 1. The schematic diagram is representing the process of synthesizing MXenes from MAX phases. Reproduced with permission from [31]. Copyright Wiley-VCH, 2014 and [32] Copyright American Chemical Society, 2012.

In essence, the chemical formula of MAX phases is $M_{n+1}AX_n$, which is defined by Barsoum [33–37]. In detail, the M element stands for transition metals from groups 3 (Sc), 4 (Ti, Zr, and Hf), 5 (V, Nb, and Ta), and 6 (Cr and Mo), the A element represents from groups 12 (Cd), 13 (Al, Ga, In, and Tl), 14 (Si, Ge, Sn, and Pb), 15 (P and As), or 16 (S), and the X element is C and/or N [33,38,39]. MXenes are generally prepared by selectively getting rid of the element of A from the parent MAX phase to form $M_{n+1}X_nT_x$ (n = 1–3), where T_x is the surface termination groups ((–O), (–F), and (–OH)) [31]. MXenes materials, which offer many advantages electronic, optical, plasmonic, and thermoelectric properties [36], have attracted much interest recently. They are currently explored for a variety of applications, including energy, environment, catalysis, photocatalysis, optical devices, electronics, biomedicals, sensors, electromagnetic, others, etc. (Figure 2) [40–43]. Among MXenes, many efforts have been devoted to promoting titanium carbide ($Ti_3C_2T_x$) as the most promising candidate of cocatalysts [44–46]. Based on the published literature dealing with MXenes, which was taken from 2011–2019 on the Web of Science, there was about 70% of researches on MXenes associated with $Ti_3C_2T_x$, as seen in the third ring of the pie chart in Figure 2 [40]. It also notes that the $Ti_3C_2T_x$ also shows a high potential to replace

the expensive Pt cocatalyst in photocatalysis. In 2017, Alhabeb et al. have provided an excellent report to give step-by-step guidance to preparing of $Ti_3C_2T_x$ by using different etchants (HF and in situ HF) and delamination methods (Figure 3a) [38]. Their corresponded scanning electron microscopy (SEM) images were obtained and shown in Figure 3b–g. For detail, Ti_3AlC_2 sample show compactly layered morphology (Figure 3b), while the morphology of the multilayered $Ti_3C_2T_x$ samples was influenced by weight percent (wt %) of HF (Figure 3c–e). On the other hand, the morphology of the multilayered NH_4–$Ti_3C_2T_x$ sample (Figure 3f) and MILD-$Ti_3C_2T_x$ sample (Figure 3g) are structurally similar to that of 5F–$Ti_3C_2T_x$ multilayered powders (Figure 3e). Theoretically, the Ti_3C_2Tx fulfill the prerequisite requirement condition for applications as catalysts for HER. It has been reported that the O and F terminated Ti_3C_2 are metallic based semiconductors with a conductivity up to 9880 S·cm^{-1}, which is higher than that of graphene [47]. This indicates that the charge transfer between Ti_3C_2 to the active site is superior to most of the reported semiconducting catalysts. Furthermore, the H* adsorption energy on the surface of Ti_3C_2 is close to 0, making it the best among noble metal free catalysts for application in HER [48]. However, most MXenes including $Ti_3C_2T_x$ are semiconductors with indirect bandgaps [49]. To apply as photocatalysts, $T_3C_2T_x$ needs to pair with other photoactive materials such as TiO_2, CdS, *g*–C_3N_4 and metal organic frameworks (MOFs). Although, the development of MXenes for wide-range application in recent years have been thoroughly summarized and discussed [34–36,49–51], a review that focuses on $Ti_3C_2T_x$ for photocatalytic HER has not been reported yet.

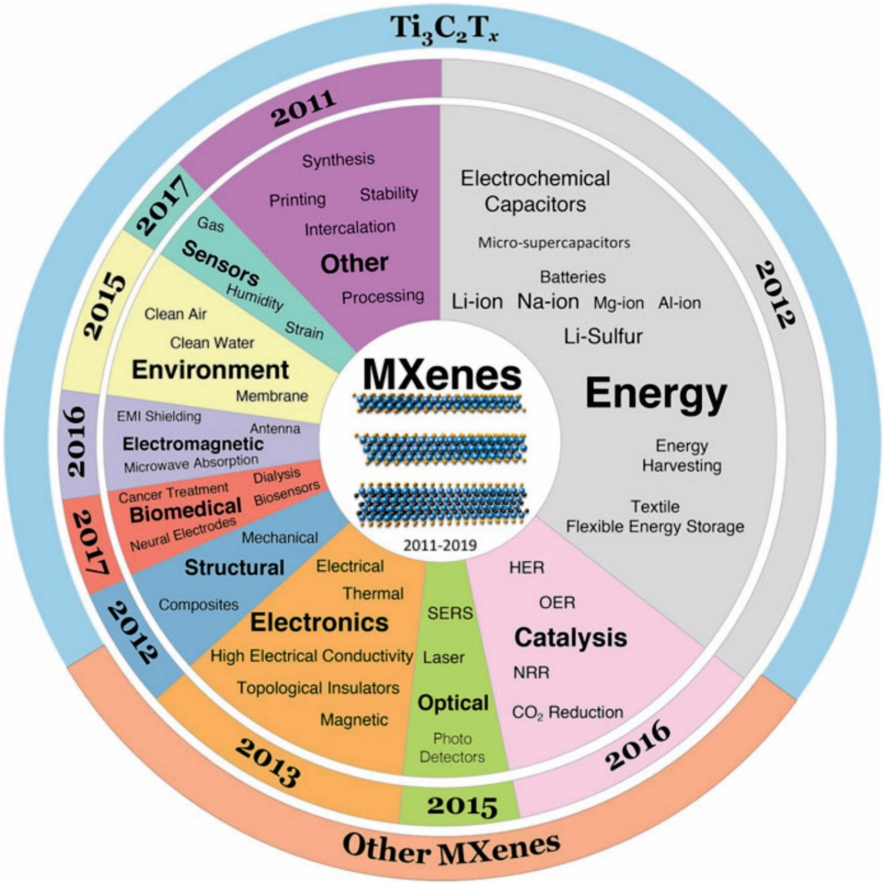

Figure 2. The general applications and properties of MXenes. The center pie chart explored the applications and properties of MXenes. The starting year in the middle pie chart ring indicates the exploration time of each application/property. The outer ring shows the ratio of publications, which were taken from 2011 to 2019 on the Web of Science, with the term of $Ti_3C_2T_x$ versus the publications deal with all MXene compositions (M_2XT_x, $M_3X_2T_x$, and $M_4X_3T_x$). Reproduced with permission from [40]. Copyright Springer Nature, 2019.

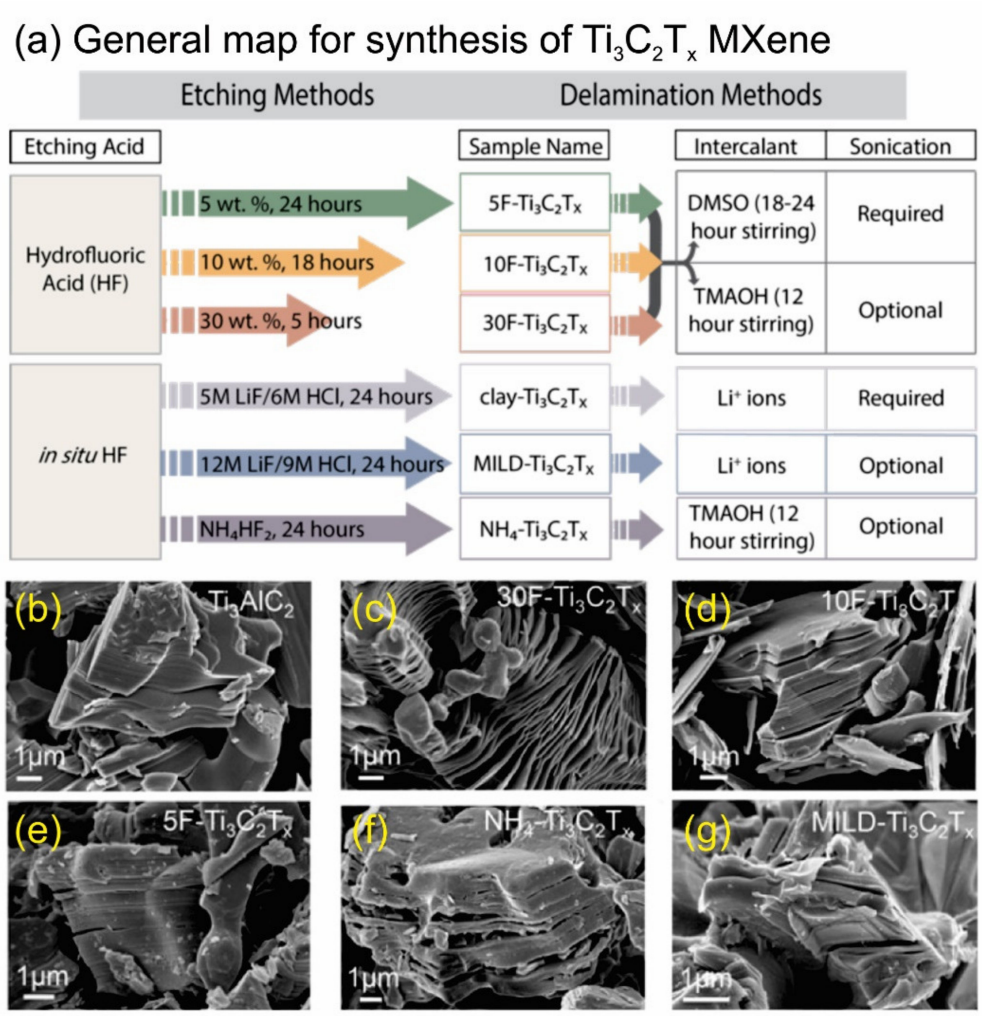

Figure 3. (**a**) The schematic diagram representing the process to prepare $Ti_3C_2T_x$ by using different etchants (HF and in situ HF) and delamination methods and (**b**–**g**) their corresponded scanning electron microscopy (SEM) images. Reproduced with permission from [37]. Copyright Royal Society of Chemistry, 2019.

In this review, we present the use of $Ti_3C_2T_x$ as the most potential and promising cocatalysts toward photocatalytic hydrogen production. Based on the recent research works, the influence on different morphology (nanotubes, nanoscrolls, quantum dots, etc.), surface termination groups (–F, –OH, and –O), and photocatalyst systems (titania (TiO_2), graphitic carbon nitride (*g*–C_3N_4) coupled Ti_3C_2 photocatalysts, etc.) are reviewed and intensified. Additionally, attention and outlook on critical challenges, prospects, and potential applications for $Ti_3C_2T_x$ cocatalysts toward sustainable solar hydrogen production are also highlighted.

2. Coupled Morphological and Structural $Ti_3C_2T_x$ Cocatalysts

Since the morphology of photocatalysts could directly influence the photocatalytic process, active sites, and charge transfer, various nanostructures of $Ti_3C_2T_x$ photocatalysts have been explored to improve the efficiency of H_2 production. However, it has not been shown yet, which types of morphology and structure of $Ti_3C_2T_x$ cocatalysts perform the best photocatalytic H_2 production rate. In this section, the photocatalytic activity over different morphological and structural $Ti_3C_2T_x$ cocatalysts was adequately highlighted and critically evaluated in terms of the H_2 production rate ($\mu mol \cdot g_{cat}^{-1} \cdot h^{-1}$) for convenient comparative purposes.

Su et al. prepared a series of $Ti_3C_2T_x/TiO_2$ composite photocatalysts with a monolayer and multilayers $Ti_3C_2T_x$ as the cocatalyst (as shown in Figure 4a) [52]. The result showed that a monolayer $Ti_3C_2T_x/TiO_2$ composite exhibited the superior H_2 production rate (2650 μmol·g_{cat}^{-1}·h^{-1}) under a 200 W Hg lamp integrated with a cutoff filter of 285–325 nm, which had more than nine-fold and two-fold higher, compared to the pure TiO_2 (290 μmol·g_{cat}^{-1}·h^{-1}) and multilayer counterpart (920 μmol·g_{cat}^{-1}·h^{-1}), respectively. The enhancement of performance is possible due to the advanced electrical conductivity of a monolayer $Ti_3C_2T_x$ and the effective charge-carrier separation at the $Ti_3C_2T_x/TiO_2$ interface. To propose a new morphology, Li et al. designed $Ti_3C_2T_x/TiO_2$ nanoflowers, which performed an outstanding H_2 production rate, compared with that of pure TiO_2 (as shown in Figure 4b) [53]. In detail, the $Ti_3C_2T_x/TiO_2$ nanoflower could reach to 526 μmol·g_{cat}^{-1}·h^{-1} in the H_2 production rate under a 300 W Xe arc lamp, which was more than four-fold higher than that of the TiO_2 nanobelts (121.82 μmol·g_{cat}^{-1}·h^{-1}). It notes that under the same experimental conditions, the H_2 production rate was 371.17 μmol·g_{cat}^{-1}·h^{-1} over the Pt/TiO_2 nanosheet. It suggests that the noble metal-free $Ti_3C_2T_x$ was considered as an alternative cocatalyst to replace the expensive and precious noble metals, such as Pt, Au, etc. To further boost the H_2 production activity, Yuan et al. prepared the $Ti_3C_2T_x$ nanofibers (NFs) structure by hydrolyzation and selective etching of Ti_3AlC_2 MAX ceramics (Figure 4c) [54]. Compared with traditional Ti_3C_2 flakes, the Ti_3C_2 NFs could provide a much higher BET (Brunauer–Emmett–Teller) surface area and expose more catalytic active sites, leading to enhanced H_2 production activity, high cycling stability, and long-term viability. Very recently, Li et al. had successfully designed $Ti_3C_2T_x$ quantum dots (QDs) by a self-assembly method, which their schematic synthesis of *g*–C_3N_4@$Ti_3C_2T_x$ QDs composites was shown in Figure 4d [55]. As expected, *g*–C_3N_4@$Ti_3C_2T_x$ QDs composites performed the best photocatalytic activity (5111.8 μmol·g_{cat}^{-1}·h^{-1}) under artificial sunlight (300 W Xe arc lamp integrated with an AM-1.5 filter), which was nearly ten-fold higher than that of *g*–$C_3N_4/Ti_3C_2T_x$ sheets (524.3 μmol·g_{cat}^{-1}·h^{-1}). Compared to the traditional $Ti_3C_2T_x$ sheets, $Ti_3C_2T_x$ QDs offered more abundant active edge sites, and excellent electronic conductivity. Additionally, the photoexcited carriers in *g*–C_3N_4@$Ti_3C_2T_x$ QDs composites could be effectively separated to rapidly take part in photocatalytic H_2 production activity, leading to enhanced photocatalytic performance efficiently. Therefore, owing to excellent physical properties, *g*–C_3N_4@$Ti_3C_2T_x$ QDs composites performed a remarkable enhancement in the photocatalytic H_2 production rate of 5111.8 μmol·g_{cat}^{-1}·h^{-1}, indicating its high potential to scale up and accelerate the H_2 production via the green photocatalysis approach.

The synthesis of different morphologies of $Ti_3C_2T_x$ cocatalysts was successfully proposed. Based on the recent studies, morphologies of $Ti_3C_2T_x$ (nanotubes, nanoscrolls, quantum dots, etc.), which might provide more BET surface area to enrich the active adsorption sites, and inhibit the recombination of e^-–h^+ pairs, resulting in effective influence to the photocatalytic activity, high cycling stability, and long-term viability.

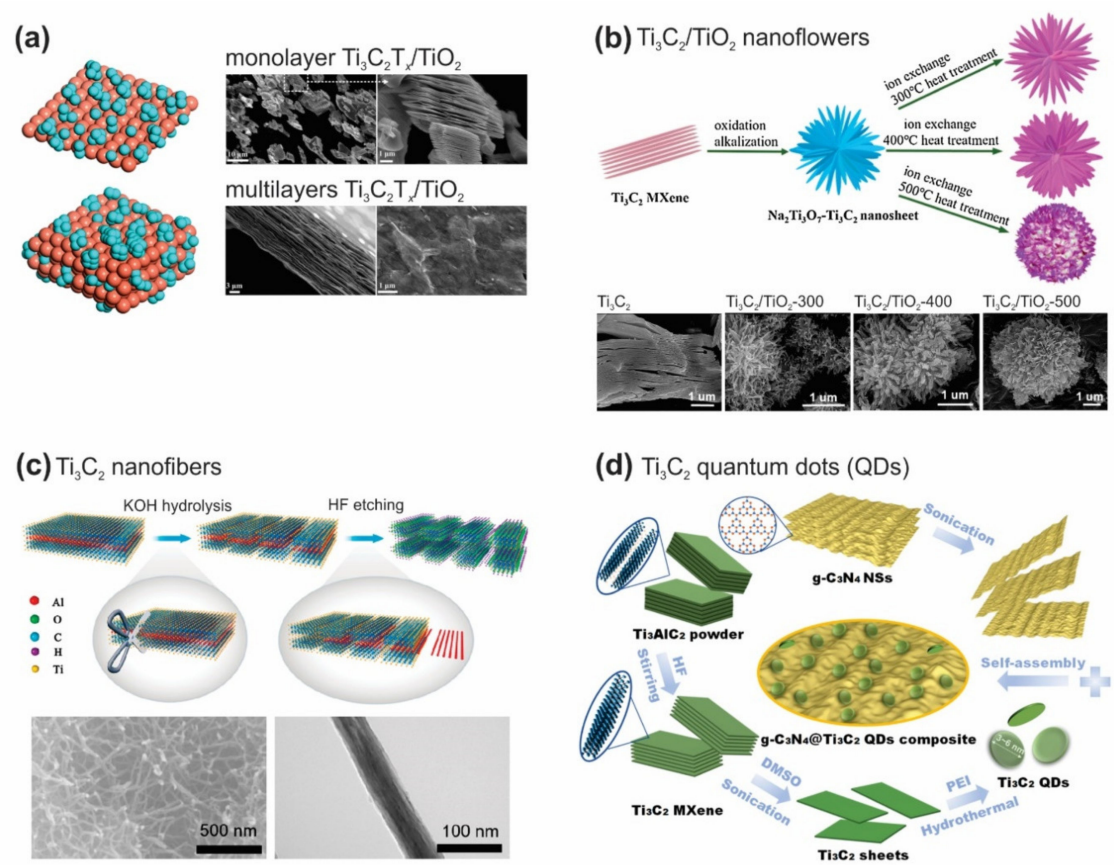

Figure 4. (**a**) Monolayer and multilayers $Ti_3C_2T_x$ as the cocatalysts. Reproduced with permission from reference [52]. Copyright American Chemical Society, 2019; (**b**) the preparation of $Ti_3C_2T_x/TiO_2$ nanoflowers and their corresponding SEM images. Reproduced with permission from ref. [53]. Copyright Nature Publishing Group, 2018; (**c**) the preparation of $Ti_3C_2T_x$ nanofibers and their corresponding SEM, TEM images. Reproduced with permission from ref. [54]. Copyright American Chemical Society, 2018; and (**d**) Schematic diagram for preparing of g–C_3N_4@$Ti_3C_2T_x$ quantum dots composites. Reproduced with permission from ref. [55]. Copyright American Chemical Society, 2019.

3. Modified $Ti_3C_2T_x$ Cocatalysts with Surface Termination Groups

In general, surface termination groups (–F, –OH, and –O) of $Ti_3C_2T_x$, which are predominantly dependent on the synthesis methods, have profoundly altered their physicochemical properties [56]. Based on theoretical calculations, many studies suggested that surface termination groups strongly influence the stability, electronic, optical, and transport properties of $Ti_3C_2T_x$ [57–60]. Due to improving the photocatalytic activity toward sustainable solar hydrogen production, there has been motivation to enhance and control the physicochemical properties of $Ti_3C_2T_x$ through surface termination groups. Li et al. found that the $Ti_3C_2T_x/TiO_2$ hybrids, which synthesized through simple calcination of F-$Ti_3C_2T_x$, exhibited potential photocatalytic activity. Its performance was two-fold higher than that of the $Ti_3C_2T_x/TiO_2$ hybrids with calcining OH-$Ti_3C_2T_x$ [37]. On the other hand, Ran et al. used density functional theory (DFT) calculations for designing and exploring the potential of novel $Ti_3C_2T_x$ nanoparticles as a promising H_2 production cocatalyst [61]. They replaced the (–F) terminations by (–O)/(–OH) terminations by the hydrothermal treatment, and found that (–O)/(–OH) terminations play a notable role for photocatalytic activity. This result was consistent with the previous finding by Sun et al. [56], who observed significant enhancement of H_2 production (88 $\mu mol \cdot g_{cat}^{-1} \cdot h^{-1}$) over O-$Ti_3C_2T_x$, compared to control samples. To further modify the surface termination groups of $Ti_3C_2T_x$, Yang et al. successfully prepared O-$Ti_3C_2T_x$/CdS hybrids through the radiofrequency oxygen plasma method (O_2/N_2, 2.2 Pa, 500 °C, 1400 W, 2.45 GHz, and 30 min), providing (a) sufficient

catching water molecules and hydrogen ions on the surface of the catalyst, and (b) stable transfer channel for electrons to repress the recombination of e^-–h^+ pairs [62]. In another approach, Xu et al. carried out a plasma treatment (N_2/H_2, atmosphere, 500 °C, 1400 W, and 30 min) for preparing layered *g*–C_3N_4/plasma-treated $Ti_3C_2T_x$ photocatalyst [63]. Based on analyzed results by Raman, FTIR, and XPS, Xu et al. observed an increase of Ti–O with a decrease of Ti–C, Ti–F, and Ti–OH. Additionally, the plasma-treated $Ti_3C_2T_x$ photocatalyst worked as an excellent acceptor of photogenerated electrons, leading to substantially reinforce the photocatalytic activity. Though the surface termination groups could be modified by several methods, such as hydrothermal treatment, simple calcination, plasma treatment, etc., more studies that elucidate the modification mechanism of surface termination groups need to be paid attention in the future.

4. The Design of $Ti_3C_2T_x$ Composite Photocatalysts

4.1. Couple with Transition Metal Oxide (TMOs)

Transition metal oxide, such as titanium dioxide (TiO_2), coupled photocatalysts have attracted dramatically increasing interest in the area of photocatalytic hydrogen generation [64–66]. Their photocatalytic activities have been markedly improved through the efforts of many research groups. However, its large bandgap and fast charge recombination limit its efficiency. To overcome this limitation, $Ti_3C_2T_x$ has been considered as promising cocatalysts for hydrogen production with TiO_2 as the photocatalyst. Zhuang has successfully prepared $TiO_2/Ti_3C_2T_x$ nanocomposites by the electrostatic self-assembly technique (Figure 5) [67]. Owing to the highly efficient separation of photogenerated carriers, which derived from the intense interfacial contact between TiO_2 nanofibers and $Ti_3C_2T_x$ nanosheets, the photocatalytic performance over $TiO_2/Ti_3C_2T_x$ nanocomposites was significantly improved. The H_2 production rate was up to 6979 $\mu mol \cdot g_{cat}^{-1} \cdot h^{-1}$ using a 10% methanol solution as the sacrificial electron donors under a 300 W Xe lamp, which was 3.8 times higher than that of pure TiO_2 nanofibers. There was no hydrogen production capacity over $Ti_3C_2T_x$ nanosheets due to its metallic character.

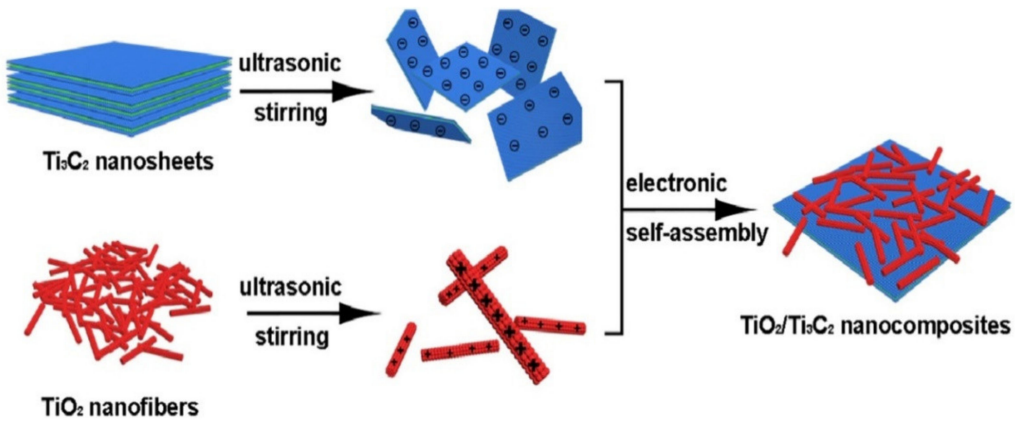

Figure 5. Schematic illustration displaying procedure for fabrication of $TiO_2/Ti_3C_2T_x$ composite. Reproduced with permission from reference [67]. Copyright Elsevier B.V., 2019.

To simplify the synthesis method, simple calcination was first proposed by Li et al. to prepare truncated octahedral bipyramidal TiO_2 (TOB-T)/$Ti_3C_2T_x$ hybrids [37]. The resultant $TiO_2/Ti_3C_2T_x$ hybrids retained the multilayer structure, and TiO_2 exhibited a truncated octahedral bipyramidal structure with exposed (001) and (101) facets. A surface heterojunction between (101) and (001) facets was established, and it could prevent the recombination of photogenerated carriers in TiO_2. Moreover, the remaining $Ti_3C_2T_x$ could act as a cocatalyst to accelerate the migration of photoinduced electrons because of its high electronic conductivity. Meanwhile, the concentration of fluorine sharply decreased during calcination, thereby reducing the toxicity and increasing the conductivity

of the samples. They pointed out that $Ti_3C_2T_x$ could enhance the photocatalytic activity of those composite photocatalysts due to the Schottky junction between $Ti_3C_2T_x$ and TiO_2 and its excellent electronic conductivity. Besides TiO_2, ZnO has also been investigated for hydrogen production [68]. It was experimentally demonstrated that the ZnO nanorods (NRs)/$Ti_3C_2T_x$ hybrids exhibited the inferior photocatalytic H_2 production activity (456 μmol·h^{-1}), while pure ZnO NRs displayed no performance [68]. However, the photocatalytic activity of the ZnO/$Ti_3C_2T_x$ composite was still much lower compared to the TiO_2/$Ti_3C_2T_x$, thus, more investigation is necessary.

4.2. Couple with Transient Metal Sulfides (TMSs)

Transition metal surface such as CdS [69–71], CdSe [72], MoS_2 [73–75], and WS_2 [76–78] has been demonstrated as potential catalysts for electrocatalytic and photocatalytic HER. Therefore, the coupling of these materials with $Ti_3C_2T_x$ might produce the composite with unprecedented performance in photocatalytic HER. As expected, Ran et al. coupled O–$Ti_3C_2T_x$ with cadmium sulfide (CdS) via a hydrothermal method to yield a composite catalyst for HER with very high performance [61]. In specific, the catalysts with the optimized composition (2.5 wt % $Ti_3C_2T_x$) can produce up to 14,342 μmol·$g_{cat}{}^{-1}$·h^{-1}, which was higher than that of Pt-CdS (10,978 μmol·$g_{cat}{}^{-1}$·h^{-1}). The HR-TEM and SEM images of the O–$Ti_3C_2T_x$ coupled CdS nanoparticles are shown in Figure 6a–b. The high photocatalytic HER performance of the O-$Ti_3C_2T_x$/CdS composite attributed to very low free energy for atomic H adsorption on the surface of O–$Ti_3C_2T_x$ (Figure 6c) and efficient charge generation and separation upon light at the interface of the composites (Figure 6d–e). Similarly, Xiao et al. coupled $Ti_3C_2T_x$ with CdS nanorod to construct a Schottky heterojunction for photocatalytic HER [79]. As a result, the CdS nanorod/$Ti_3C_2T_x$ nanosheet exhibited a performance 7-fold higher than that of pristine CdS [79]. The improvement was postulated to originate from the synergistic effect between the CdS nanorod and $Ti_3C_2T_x$ nanosheets that improves light absorption, charge separation, and conductivity of the composite catalysts. Tie et al. decorated ZnS nanoparticles with $Ti_3C_2T_x$ nanosheets to yield photocatalytic HER with a production rate of 502.6 μmol·$g_{cat}{}^{-1}$·h^{-1} under optimal conditions, is almost 4-fold higher than pure ZnS (124.6 μmol·$g_{cat}{}^{-1}$·h^{-1}) [80]. Besides, the alloy transition metal sulfide/$Ti_3C_2T_x$ was also investigated. For example, Cheng et al. demonstrated a high-performance composite for photocatalytic HER composed of $CdLa_2S_4$ and $Ti_3C_2T_x$ nanocomposite [81]. In specific, these composite nanomaterials yield photocatalytic HER with the H_2 production rate of 11,182.4 μmol·$g_{cat}{}^{-1}$·h^{-1}, and apparent quantum efficiency reached 15.6% at 420 nm. The performance of $CdLa_2S_4$/$Ti_3C_2T_x$ nanocomposite, therefore, improves the production rate up to 13.4 times compared to that of pristine $CdLa_2S_4$ and even higher than that of Pt/$CdLa_2S_4$. To sum up, $Ti_3C_2T_x$ couple with TMSs could reach to a desirable level. In detail, 2.5 wt % $Ti_3C_2T_x$/CdS and ZnS/$Ti_3C_2T_x$ nanosheets exhibited very attractive photocatalytic activity, making them good candidates for photocatalytic HER.

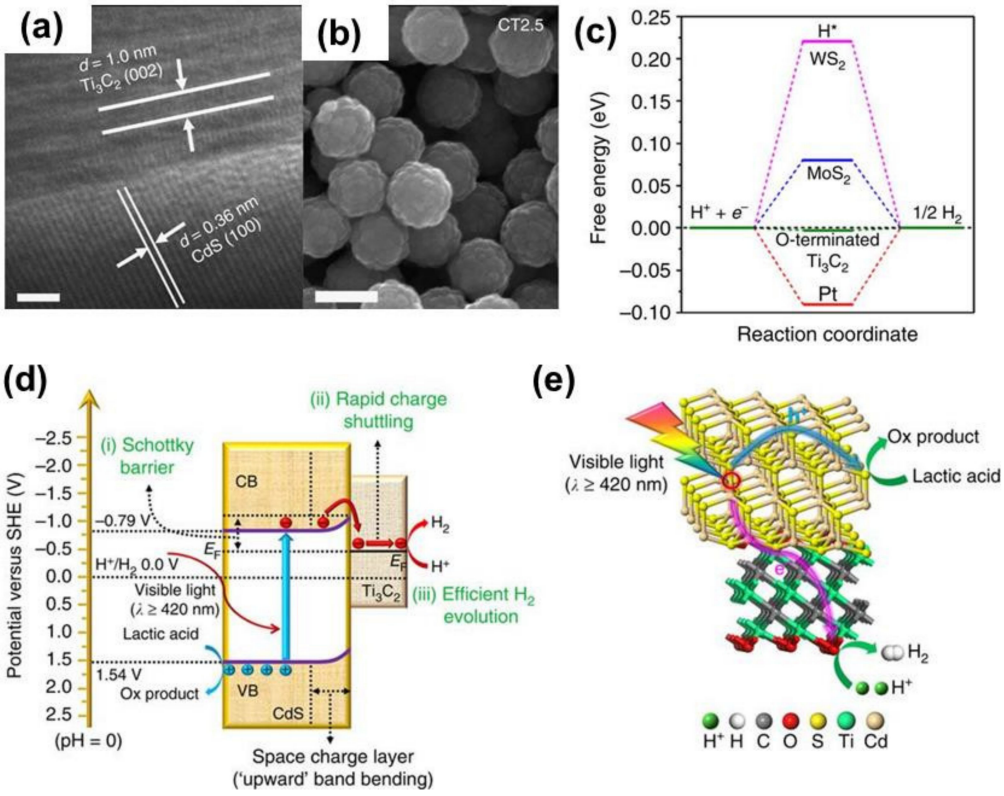

Figure 6. (**a**,**b**), TEM and SEM images of $Ti_3C_2T_x$/CdS composite structure; (**c**) the calculated free-energy band diagram of HER with different catalysts including MoS_2, WS_2, and O-$Ti_3C_2T_x$; (**d**) band diagram of $Ti_3C_2T_x$/CdS showing the charge separation and transferring from CdS to $Ti_3C_2T_x$ for HER; and (**e**) the proposed mechanism of HER over $Ti_3C_2T_x$/CdS composite. Reproduced with permission from reference [61]. Copyright Nature Publishing Group, 2017.

4.3. Couple with the Metal–Organic Framework

MOFs and their derivative have been emerging as efficient catalysts for photo electrocatalytic HER. The first combination of $Ti_3C_2T_x$/MOFs composite was reported by Tian et al. in 2019 [82]. The TEM images in Figure 7a,b indicated that the MOFs were well connected with the MOFs. As a result, the $Ti_3C_2T_x$/MOFs composite displays photocatalytic activity better than the Pt decorated MOFs (2 wt % Pt/UiO-66-NH_2). The performance of $Ti_3C_2T_x$/MOFs can be observed in Figure 7c. The schematic illustration of energy band alignment between $Ti_3C_2T_x$ and MOFs is shown in Figure 7d. Under sunlight irradiation, the electron-hole pairs were generated in MOFs. Owing to the good contact and conductivity, the photo-induced electron can be easily transferred to the $Ti_3C_2T_x$ surface to participate in the HER, thus, improving the overall performance of the composite catalysts.

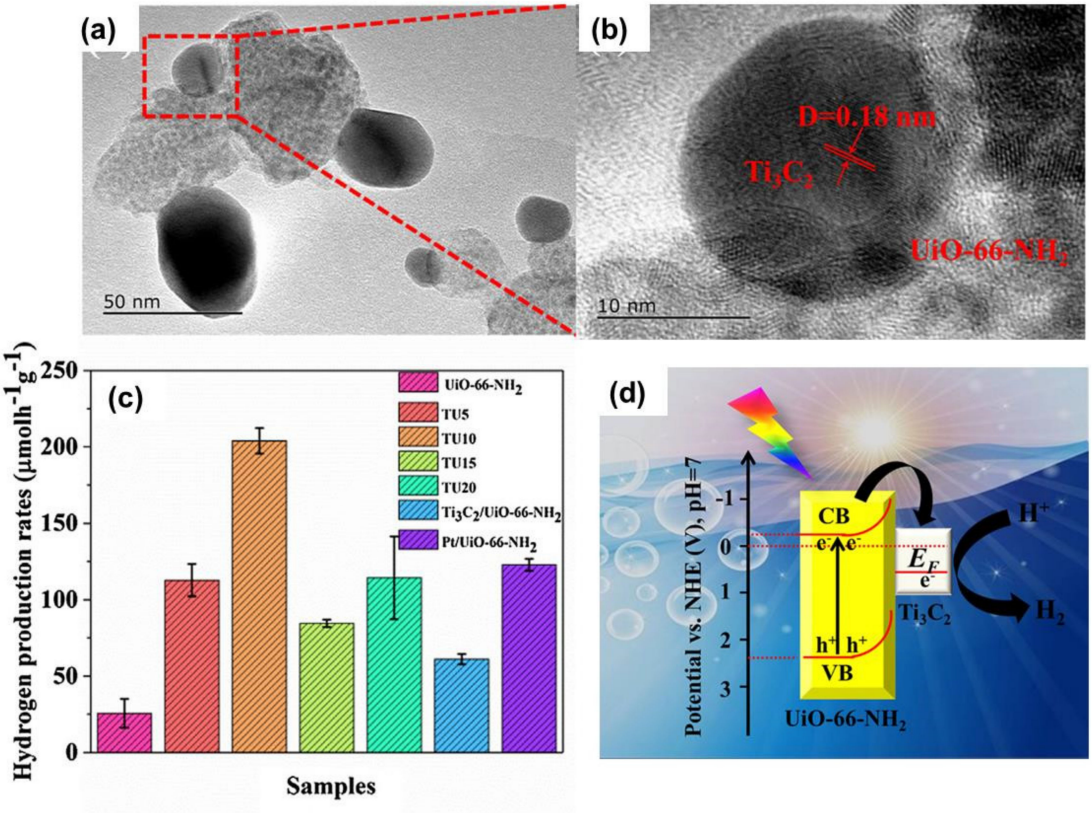

Figure 7. (**a**,**b**)TEM images presented the formation of $Ti_3C_2T_x$ and Zr-MOFs heterostructure; (**c**) Hydrogen production rates of $Ti_3C_2T_x$/Zr-MOF with different concentrations of $Ti_3C_2T_x$; (**d**) Energy band diagram of $Ti_3C_2T_x$/Zr-MOF for photocatalytic HER. Reproduced with permission from reference [82]. Copyright Elsevier B.V., 2019.

4.4. Coupled with Graphitic Carbon Nitride (g–C_3N_4)

Graphitic carbon nitride (*g*–C_3N_4) coupled photocatalysts have attracted dramatically increasing interest in the area of visible-light-induced photocatalytic hydrogen generation due to the unique electronic band structure and high thermal and chemical stability of *g*–C_3N_4 [83–85]. Besides, the work had been done by Li et al. in the previous section, *g*–C_3N_4@$Ti_3C_2T_x$ QDs [55], another study that couples $Ti_3C_2T_x$/g–C_3N_4 has also been reported. Typically, Su et al. constructed a heterojunction using $Ti_3C_2T_x$ and *g*–C_3N_4 nanosheets via the electrostatic self-assembly method [86]. A small amount of $Ti_3C_2T_x$ was loaded onto *g*–C_3N_4, with a concentration that ranged from 1% to 5%. Interestingly, the $Ti_3C_2T_x$/*g*–C_3N_4 exhibits significantly improved photocatalytic activity towards HER compared to that of pristine *g*–C_3N_4 [86]. Instead of using pristine *g*–C_3N_4, Lin et al. used O-doped *g*–C_3N_4 to form the heterostructure with $Ti_3C_2T_x$ to improve the H_2 production rate of catalysts two-fold [87]. The fabrication process for constructing $Ti_3C_2T_x$/O-doped *g*–C_3N_4 is shown in Figure 8a. The SEM and TEM images in Figure 8b–d indicates that well interspersed $Ti_3C_2T_x$/O-doped g–C_3N_4 heterostructure was obtained. As a result, the $Ti_3C_2T_x$/O-doped *g*–C_3N_4 yield H_2 with a production rate of 25,124 $\mu mol \cdot g_{cat}^{-1} \cdot h^{-1}$, whereas, pristine O-doped *g*–C_3N_4 and $Ti_3C_2T_x$/pristine *g*–C_3N_4 exhibit a lower H_2 generation rate of 13,745 and 15,573 $\mu mol \cdot g_{cat}^{-1} \cdot h^{-1}$, respectively. Figure 8e indicates that the electron from O-doped *g*–C_3N_4 can be easily transferred to $Ti_3C_2T_x$ for the HER. These results suggested that *g*–C_3N_4 is a very good photoactive material to pair with $Ti_3C_2T_x$ to yield efficient photocatalytic HER. However, the research related to this topic is still very limited, thus it needs more investigation in the near future.

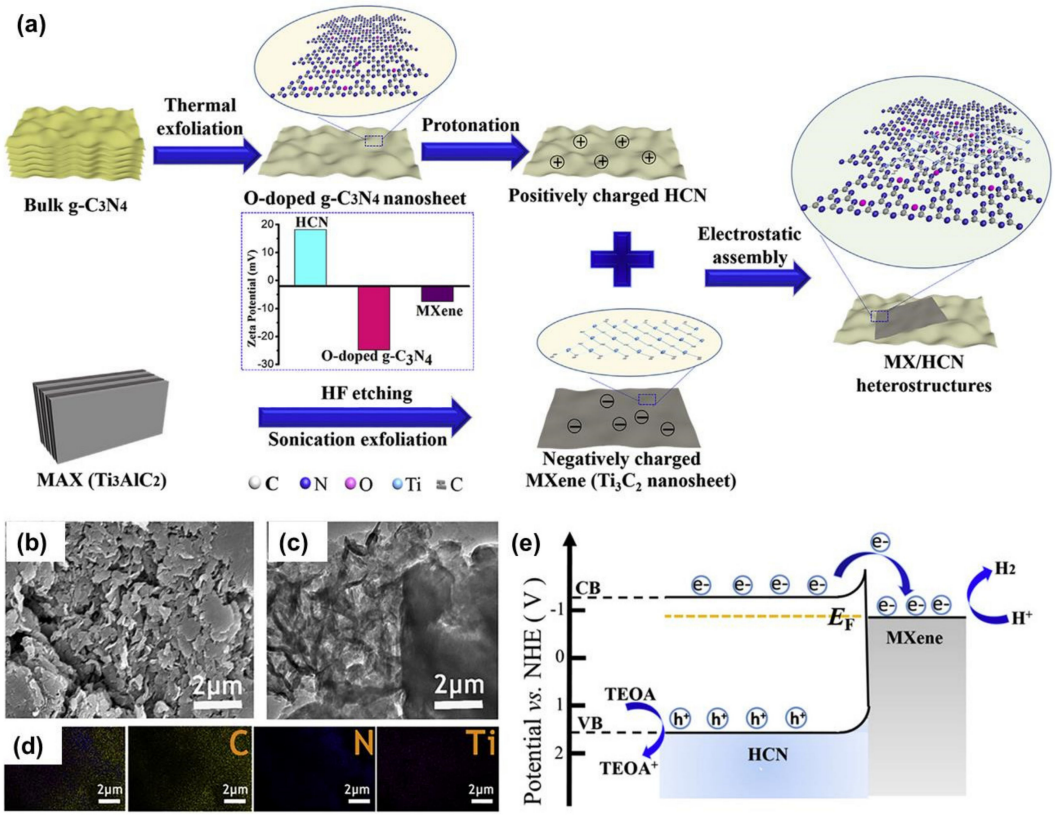

Figure 8. (**a**) Fabrication process of the $Ti_3C_2T_x$/O-doped *g*–C_3N_4 heterostructure. (**b**–**d**) SEM images, TEM images, and EDS spectra of $Ti_3C_2T_x$/O-doped *g*–C_3N_4. (**e**) The working mechanism of $Ti_3C_2T_x$/O-doped *g*–C_3N_4 photocatalyst. Reproduced with permission from reference [87]. Copyright Elsevier B.V., 2019.

4.5. Ternary Composites

Apart from binary composites, ternary composites of $Ti_3C_2T_x$ have also been rationally developed. To obtain the ternary composite catalyst, Tial et al. first introduced TiO_2 onto the surface of $Ti_3C_2T_x$ via thermal annealing at 600 °C under N_2 atmosphere [88]. After that, the Zr–MOF (UiO-66-NH_2) was growth on $Ti_3C_2T_x/TiO_2$ using a facile hydrothermal approach. The schematic illustration of the synthesis procedure is shown in Figure 9a. The TEM displaying the ternary phase of the composite is presented in Figure 9b. It can be observed that the ternary structure was well established. As a consequence, the ternary composite ($Ti_3C_2T_x/TiO_2$/UIO-66-NH_2) exhibited a performance two times higher than that of the binary composite ($Ti_3C_2T_x$/UIO-66-NH_2). The improvement in the catalytic activity of the $Ti_3C_2T_x/TiO_2$/UIO-66-NH_2) not only comes from the improvement of the light absorption by using a double light absorber (TiO_2/UIO-66-NH_2) but also the enhancement of the charge separation of collection efficiency. The working mechanism of the binary and ternary composite was clearly illustrated in Figure 9c. Additionally, by taking advantage of the ternary composites with the composition of $Mo_xS/TiO_2/Ti_3C_2T_x$, Li et al. improved the H_2 production rate up to 10,505.8 μmol·g_{cat}^{-1}·h^{-1}, which was 193 times compared to that of pristine TiO_2 [46]. Similarly, many other ternary composites have been constructed with excellent photocatalytic activity towards HER such as $Mo_xS@TiO_2@Ti_3C_2T_x$ [46], Cu/$TiO_2@Ti_3C_2T_x$ [89], 1T–$MoS_2/Ti_3C_2T_x/TiO_2$ [90], 1T–$WS_2@TiO_2@Ti_3C_2T_x$ [91], Cu_2O/(001)/$TiO_2/Ti_3C_2T_x$ [92], $Ti_3C_2T_x/TiO_2$/*g*–C_3N_4 [93], *g*–$C_3N_4/Ti_3C_2T_x$/Pt [45], CdS/$MoS_2/Ti_3C_2T_x$ [94], and $TiO_2/Ti_3C_2T_x/CoS_x$ [95]. However, it is noted that a multicomponent photocatalytic hybrid composed of MXene with other cocatalysts are still in an early stage and requires further efforts.

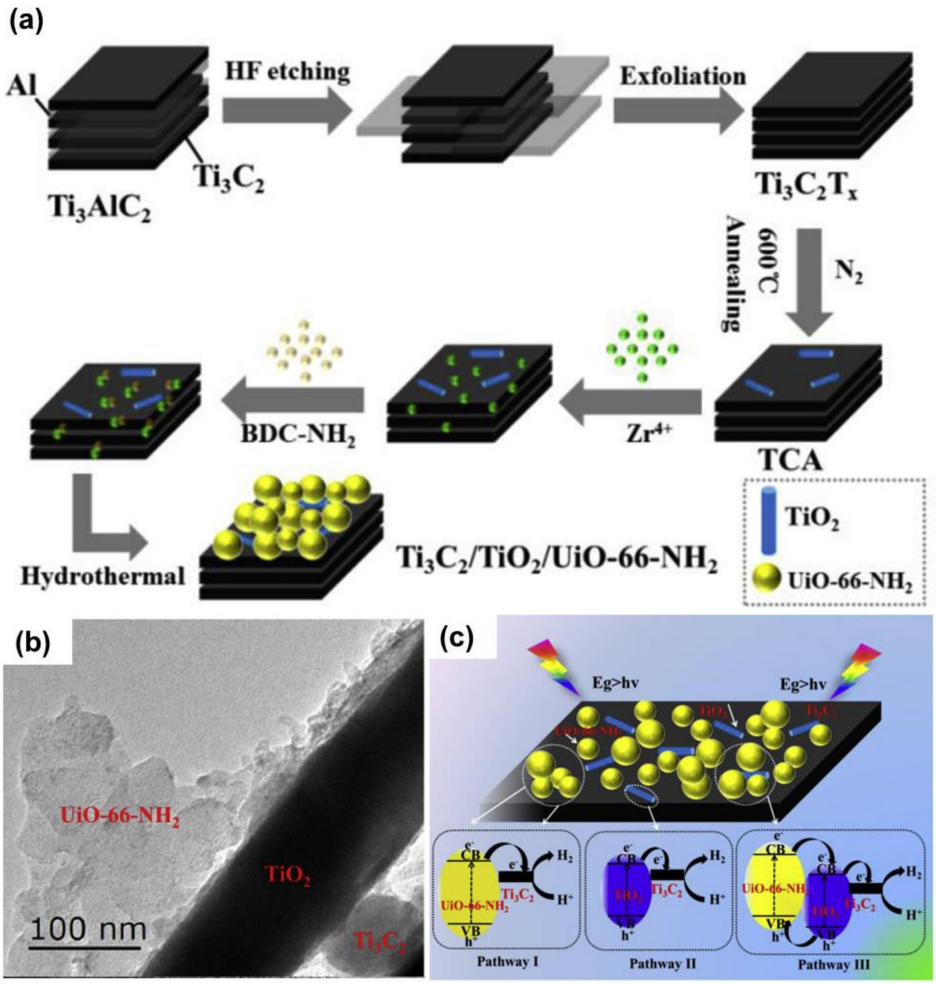

Figure 9. (**a**) Route for the synthesis of $Ti_3C_2T_x/TiO_2$/UiO-66-NH_2 ternary composite, (**b**) TEM image of the $Ti_3C_2T_x/TiO_2$/UiO-66-NH_2 ternary composite, and (**c**) working mechanism of ternary composite photocatalyst for HER. Reproduced with permission from reference [88]. Copyright Elsevier B.V., 2019.

5. Comparison of the Photocatalytic Hydrogen Production

To sum up, a detailed summary and comparison of recently reported $Ti_3C_2T_x$ cocatalysts toward photocatalytic hydrogen production are given in Table 1. Although the experimental reaction conditions were different, we compared the photocatalytic activity in terms of the H_2 evolution rate. Then, all the evolution rate of H_2 were obtained and transformed into a logical unit ($\mu mol \cdot g_{cat}^{-1} \cdot h^{-1}$) for acceptable comparative purposes. We found that $Ti_3C_2T_x$/O-doped *g*–C_3N_4 achieved interest in the H_2 evolution rate (25,124 $\mu mol \cdot g_{cat}^{-1} \cdot h^{-1}$). To further understand the photocatalytic activity of MXenes, a broad comparison was collected for different types of MXenes (as shown in Table 2). In addition to $Ti_3C_2T_x$, only a few studies using other types of MXenes cocatalysts, such as Nb_2CT_x [96] and Ti_2C [97], for hydrogen production. Interestingly, the hybrid composite of $Zn_{0.5}Cd_{0.5}S$ and Ti_2C/TiO_2 exhibited an attractive H_2 production rate (32,560 $\mu mol \cdot g_{cat}^{-1} \cdot h^{-1}$) [97]. This photocatalytic enhancement might be contributed by the effective light absorption and the efficient separation of electron-hole pairs.

Table 1. Photocatalytic hydrogen production over $Ti_3C_2T_x$ cocatalysts.

No.	Photocatalysts	Light Source	Reaction Temp.	Scavenger	Reactant Medium	H_2 Production Rate ($\mu mol \cdot g_{cat}^{-1} \cdot h^{-1}$)	Ref/(Year)
1	TiO_2 nanofibers/ $Ti_3C_2T_x$ nanosheets (3 wt %)	300 W Xe lamp	Room temperature (RT)	Methanol	CH_3OH/H_2O (*l*, 1:9)	6979	[67]/2019
2	TiO_2 nanofibers					1831	
3	$Ti_3C_2T_x$ nanosheets					ND	
4	F–$Ti_3C_2T_x/TiO_2$ hybrids	350 W Xe arc lamp	RT	Glycerin	$C_3H_8O_3/H_2O$ (*l*, 1:9)	127.1	[37]/2019
5	OH–$Ti_3C_2T_x/TiO_2$ hybrids					61.4	
6	CdS (CT0)	300 W Xe arc lamp: $\lambda \geq 420$ nm; 80 mW·cm^{-2}	RT	Lactic acid	$C_3H_6O_3/H_2O$ (*l*, 17.6:62.4)	105	[61]/2017
7	$Ti_3C_2T_x$ nanoparticles					ND	
8	0.05 wt % $Ti_3C_2T_x$ nanoparticles/CdS (CT0.05)					993	
9	0.1 wt % $Ti_3C_2T_x$ nanoparticles/CdS (CT0.1)					1278	
10	2.5 wt % $Ti_3C_2T_x$ nanoparticles/CdS (CT2.5)					14,342	
11	5 wt %$Ti_3C_2T_x$ nanoparticles/CdS (CT5)					3377	
12	Pt/CdS					10,978	
13	NiS/CdS					12,953	
14	Ni/CdS					8649	
15	MoS_2/CdS					6183	
16	$Ti_3C_2T_x$ nanosheets modified Zr–MOFs (UiO-66-NH_2)	350 W Xe lamp	RT	S^{2-}/SO_3^{2-}	0.1 M Na_2S and 0.1 M Na_2SO_3	204	[82]/2019
17	2 wt % Pt/UiO-66-NH_2					123	
18	UiO-66-NH_2					25.6	
19	$Zn_2In_2S_5/Ti_3C_2T_x$ hybrids	300 W Xe arc lamp: $\lambda \geq 420$ nm;	RT	S^{2-}/SO_3^{2-}	0.35 M Na_2S and 0.25 M Na_2SO_3	2596.8	[92]/2019
20	$Ti_3C_2T_x/TiO_2$/UiO-66-NH_2 hybrid	300 W Xe lamp (PerkinElmer): $350 < \lambda < 780$ nm	5 °C	S^{2-}/SO_3^{2-}	0.1 M Na_2S and 0.1 M Na_2SO_3	1980	[88]/2019
21	$Ti_3C_2T_x$/UiO-66-NH_2					1320	
22	UiO-66-NH_2					942.9	
23	MoxS@TiO_2@$Ti_3C_2T_x$ composite	300 W Xe arc lamp: an AM1.5 filter; 180 mW·cm^{-2} within a range of 200–1200 nm.	25 °C	Triethanolamine (TEOA)	TEOA in aqueous acetone	10505.8	[46]/2020
24	Cu/TiO_2@$Ti_3C_2T_x$	300W Xe lamp (CEL-HXF 300E)	RT	Methanol	CH_3OH/H_2O (*l*, 1:14)	764	[89]/ 2018
25	TiO_2@$Ti_3C_2T_x$					65	
26	1T–MoS_2 nanopatch/$Ti_3C_2T_x/TiO_2$ nanosheet	300 W Xe arc lamp: an AM1.5 filter; 180 mW·cm^{-2} within a range of 200–1200 nm.	25 °C	TEOA	TEOA/Acetone/H_2O (*l*, 1:3:16)	9738	[90]/2019
27	$Ti_3C_2T_x/TiO_2$ nanosheet					898	
28	TiO_2 nanosheet					74	
29	1T–WS_2@TiO_2@ $Ti_3C_2T_x$	300 W Xe arc lamp: an AM-1.5 filter	25 °C	TEOA	TEOA/Acetone/H_2O (*l*, 1:3:16)	3409.8	[91]/2019
30	TiO_2					67.8	
31	ternary Cu_2O/(001) TiO_2@$Ti_3C_2T_x$	300 W Xe lamp (CEL-HXF 300E)	RT	Methanol	CH_3OH/H_2O (*l*, 1:14)	1496	[92]/2019
32	(001) TiO_2@ $Ti_3C_2T_x$					165	
33	$Ti_3C_2T_x$@TiO_2@MoS_2 composites	300 W Xe arc lamp (CELHXF300): an AM1.5 filter	25 °C	TEOA	TEOA in aqueous acetone	6425.3	[95]/2019
34	$Ti_3C_2T_x$@TiO_2					898.1	
35	$TiO_2/Ti_3C_2T_x$/CoS	300 W Xe arc lamp	RT	Methanol	CH_3OH/H_2O (*l*, 1:4)	950	[95]/2019
36	TiO_2					140	
37	CoS					10	
38	$TiO_2/Ti_3C_2T_x$					330	
39	TiO_2/CoS					540	
40	*g*–$C_3N_4/Ti_3C_2T_x$/Pt	300 W Xe arc lamp	RT	TEOA	TEOA/H_2O (*l*, 1:9)	5100	[45]/2018
41	*g*–$C_3N_4/Ti_3C_2T_x$					1700	
42	*g*–C_3N_4/Pt					1275	
43	*g*–C_3N_4@$Ti_3C_2T_x$ quantum dots	300 W Xe arc lamp (CELHXF300): an AM-1.5 filter	RT	TEOA	TEOA/H_2O (*l*, 3:17)	5111.8	[55]/2019
44	*g*–C_3N_4					196.8	
45	Pt/*g*–C_3N_4					1896.4	

Table 1. *Cont.*

46	$Ti_3C_2T_x$/O-doped *g*–C_3N_4	300 W Xe lamp	RT	TEOA	TEOA (*l*)	25,124	[87]/2019
47	O-doped *g*–C_3N_4					13,745	
48	$Ti_3C_2T_x$/*g*–C_3N_4					15,573	
49	$Ti_3C_2T_x$/TiO_2/*g*–C_3N_4 nanocomposites	300 W Xe lamp: λ > 420 nm	25 °C	TEOA	TEOA/H_2O (*l*, 2:17)	1620	[93]/2018
50	*g*–C_3N_4					670	
51	$CdLa_2S_4$/$Ti_3C_2T_x$ nanocomposite	300 W Xe lamp: a high-pass filter (λ > 420 nm)	RT	S^{2-}/SO_3^{2-}	0.35 M Na_2S and 0.25 M Na_2SO_3	11,182.4	[81]/2019
52	Pt/$CdLa_2S_4$					1734.7	
53	$CdLa_2S_4$					832	
54	$Ti_3C_2T_x$					ND	
55	CdS nanorod/ $Ti_3C_2T_x$ nanosheet	300 W Xe lamp (PerkinElmer): a cut-off filter (λ > 420 nm)	6 °C	Lactic acid	$C_3H_6O_3/H_2O$ (*l*, 1:9)	2407	[79]/2019
56	CdS nanorod					360	
57	ZnS nanoparticles/$Ti_3C_2T_x$ nanosheets	300 W Xe lamp	RT	Lactic acid	$C_3H_6O_3/H_2O$ (*l*, 1:4)	502.6	[80]/2019
58	ZnS nanoparticles					124.6	
59	ZnO nanorods /$Ti_3C_2T_x$ hybrids	300 W Xe lamp: λ > 420 nm	RT	Ethanol	C_2H_5OH/H_2O (*l*, 3:16)	456	[68]/2020
60	ZnO nanorods					ND	
61	CdS/MoS_2/$Ti_3C_2T_x$ composites	300 W Xe lamp (CELHXF300): a cut-off filter (λ > 420 nm)	RT	S^{2-}/SO_3^{2-}	0.25 M Na_2S and 0.35 M Na_2SO_3	9679	[94]/2019
62	plasma-$Ti_3C_2T_x$/CdS hybrids	300 W arc Xe lamp (PLSSXE300): a UV cut-off filter (λ > 420 nm);	RT	Lactic acid	$C_3H_6O_3/H_2O$ (*l*, 1:9)	825	[62]/2019
63	$Ti_3C_2T_x$/CdS hybrids					473	
64	*g*–C_3N_4/plasma-$Ti_3C_2T_x$	350 W Xe lamp: a UV cut-off filter (λ > 400 nm); 70 mW·cm^{-2}	RT	TEOA	TEOA/H_2O (*l*, 1:9)	17.8	[63]/2020
65	*g*–C_3N_4/$Ti_3C_2T_x$					7.5	
66	*g*–C_3N_4					0.7	
67	TiO_2/$Ti_3C_2T_x$@AC-48 h composite	350 W Xe lamp (AHD 350): a cut-off filter (λ > 400 nm)	RT	Ascorbic acid (AA)	29 mg·mL^{-1} AA with the sensitization of 1 mM EY in aqueous solution	33.4	[98]/2019
68	1% Pt/TiO_2					0.7	
69	TiO_2/$Ti_3C_2T_x$@AC-48 h composite				29 mg·mL^{-1} AA in aqueous solution	0.3	

Table 2. Photocatalytic hydrogen production over selected MXenes cocatalysts.

No.	Photocatalysts	Light Source	Reaction Temp.	Scavenger	Reactant Medium	H_2 Production Rate (μmol·g_{cat}^{-1}·h^{-1})	Ref./(Year)
1	$Ti_3C_2T_x$/O-doped *g*–C_3N_4	300 W Xe lamp	RT	TEOA	TEOA (*l*)	25,124	[87]/2019
2	$CdLa_2S_4$/$Ti_3C_2T_x$ nanocomposite	300 W Xe lamp: a high-pass filter (λ > 420 nm)	RT	S^{2-}/SO_3^{2-}	0.35 M Na_2S and 0.25 M Na_2SO_3	11,182.4	[81]/2019
3	2.5 wt % $Ti_3C_2T_x$ nanoparticles/CdS (CT2.5)	300 W Xe arc lamp: λ ≥ 420 nm; 80 mW·cm^{-2}	RT	Lactic acid	$C_3H_6O_3/H_2O$ (*l*, 17.6:62.4)	14,342	[61]/2017
4	Nb_2O_5/C/Nb_2CT_x Composites	200 W Hg lamp: λ = 285–325 nm; 120 mW·cm^{-2}	25 °C	Methanol	CH_3OH/H_2O (*l*, 1:3)	7.81	[96]/2018
5	$Zn_{0.5}Cd_{0.5}S$/Ti_2C/TiO_2	300 W Xe lamp: λ ≥ 400 nm;	RT	S^{2-}/SO_3^{2-}	0.3 M Na_2S and 0.3 M Na_2SO_3	32,560	[97]/2020

6. Summary and Perspectives

In conclusion, $Ti_3C_2T_x$ exhibited excellent catalytic properties toward photocatalytic HER. However, the property of $Ti_3C_2T_x$ was strongly affected by its surface functional groups and coupled materials. Specifically, the O terminated $Ti_3C_2T_x$ offered the best catalytic activity. The performance of $Ti_3C_3T_x$ could also be improved by paring with other photoactive materials such as TiO_2, ZnO, MoS_2, WS_2, CdS, and graphitic carbon nitride. The composite materials not only improved light absorption but also enhanced the charge separation and active sites. Thus improving the overall performance $Ti_3C_2T_x$ under UV-vis light irradiation. Nonetheless, there were still limitations that hinder the application of $Ti_3C_2T_x$ for practical applications such as scalability and stability. The future development of $Ti_3C_2T_x$ as photocatalysts can be extended into the following directions: (1) developing a novel method for production of $Ti_3C_2T_x$ in large scale at a mild condition such as a lower temperature, less toxic etchant, and solution-processable; (2) constructing novel functional groups on the surface of $Ti_3C_2T_x$ for improving the catalytic properties; (3) designing novel materials to couple with $Ti_3C_2T_x$

for further enhancing the photocatalytic activity such as oxide perovskite and halide perovskite can be considered; and (4) improving the stability of $Ti_3C_2T_x$ for improving the lifetime of catalysts under working through structural engineering or passivation.

Author Contributions: V.-H.N, S.Y.K, and Q.V.L conceived the idea and supervised the project. All authors wrote and approved the final version of the manuscript. All authors have read and agreed to the published version of the manuscript.

Funding: This research was supported by the Creative Materials Discovery Program through the NRF funded by the Ministry of Science and ICT (grant number 2017M3D1A1039379) and the Basic Research Laboratory of the NRF funded by the Korean government (grant number 2018R1A4A1022647). The authors gratefully acknowledge Lac Hong University, Vietnam for the financial and equipment support under grant number LHU-RF-TE-18-01-09.

Conflicts of Interest: The authors declare no conflict of interest

References

1. Bockris, J. *Energy: The Solar-Hydrogen Alternative*; Halsted Press: New York, NY, USA, 1975; 381p.
2. Huang, C.-W.; Nguyen, B.-S.; Wu, J.C.S.; Nguyen, V.-H. A current perspective for photocatalysis towards the hydrogen production from biomass-derived organic substances and water. *Int. J. Hydrog. Energy* **2019**. [CrossRef]
3. Nguyen, T.P.; Nguyen, D.L.T.; Nguyen, V.-H.; Le, T.-H.; Ly, Q.V.; Vo, D.-V.N.; Nguyen, Q.V.; Le, H.S.; Jang, H.W.; Kim, S.Y.; et al. Facile synthesis of WS_2 hollow spheres and their hydrogen evolution reaction performance. *Appl. Surf. Sci.* **2020**, *505*, 144574. [CrossRef]
4. Tekalgne, M.A.; Nguyen, K.V.; Nguyen, D.L.T.; Nguyen, V.-H.; Nguyen, T.P.; Vo, D.-V.N.; Trinh, Q.T.; Hasani, A.; Do, H.H.; Lee, T.H.; et al. Hierarchical molybdenum disulfide on carbon nanotube–reduced graphene oxide composite paper as efficient catalysts for hydrogen evolution reaction. *J. Alloys Compd.* **2020**, *823*, 153897. [CrossRef]
5. Nguyen, T.P.; Kim, S.Y.; Lee, T.H.; Jang, H.W.; Le, Q.V.; Kim, I.T. Facile synthesis of $W_2C@WS_2$ alloy nanoflowers and their hydrogen generation performance. *Appl. Surf. Sci.* **2020**, *504*, 144389. [CrossRef]
6. Tekalgne, M.A.; Hasani, A.; Heo, D.Y.; Van Le, Q.; Nguyen, T.P.; Lee, T.H.; Ahn, S.H.; Jang, H.W.; Kim, S.Y. $SnO_2@WS_2$/p-Si Heterostructure Photocathode for Photoelectrochemical Hydrogen Production. *J. Phys. Chem. C* **2020**, *124*, 647–652. [CrossRef]
7. Hasani, A.; Le, Q.V.; Tekalgne, M.; Choi, M.-J.; Lee, T.H.; Jang, H.W.; Kim, S.Y. Direct synthesis of two-dimensional MoS_2 on p-type Si and application to solar hydrogen production. *NPG Asia Mater.* **2019**, *11*, 47. [CrossRef]
8. Hasani, A.; Van Le, Q.; Tekalgne, M.; Choi, M.-J.; Choi, S.; Lee, T.H.; Kim, H.; Ahn, S.H.; Jang, H.W.; Kim, S.Y. Fabrication of a WS_2/p-Si Heterostructure Photocathode Using Direct Hybrid Thermolysis. *ACS Appl. Mater. Interfaces* **2019**, *11*, 29910–29916. [CrossRef] [PubMed]
9. Tekalgne, M.; Hasani, A.; Le, Q.V.; Nguyen, T.P.; Choi, K.S.; Lee, T.H.; Jang, H.W.; Luo, Z.; Kim, S.Y. CdSe Quantum Dots Doped WS_2 Nanoflowers for Enhanced Solar Hydrogen Production. *Phys. Status Solidi A Appl. Res.* **2019**, *216*, 1800853. [CrossRef]
10. Tekalgne, M.; Hasani, A.; Van Le, Q.; Kim, S.Y. Transition metal dichalcogenide-based composites for hydrogen production. *Funct. Compos. Struct.* **2019**, *1*, 012001. [CrossRef]
11. Guo, W.; Le, Q.V.; Do, H.H.; Hasani, A.; Tekalgne, M.; Bae, S.-R.; Lee, T.H.; Jang, H.W.; Ahn, S.H.; Kim, S.Y. $Ni_3Se_4@MoSe_2$ Composites for Hydrogen Evolution Reaction. *Appl. Sci.* **2019**, *9*, 5035. [CrossRef]
12. Hasani, A.; Tekalgne, M.; Le, Q.V.; Jang, H.W.; Kim, S.Y. Two-dimensional materials as catalysts for solar fuels: hydrogen evolution reaction and CO_2 reduction. *J. Mater. Chem. A* **2019**, *7*, 430–454. [CrossRef]
13. Guo, W.; Le, Q.V.; Hasani, A.; Lee, T.H.; Jang, H.W.; Luo, Z.; Kim, S.Y. $MoSe_2$-GO/rGO Composite Catalyst for Hydrogen Evolution Reaction. *Polymers* **2018**, *10*, 1309. [CrossRef]
14. Nguyen, T.P.; Le, Q.V.; Choi, S.; Lee, T.H.; Hong, S.-P.; Choi, K.S.; Jang, H.W.; Lee, M.H.; Park, T.J.; Kim, S.Y. Surface extension of MeS_2 (Me = Mo or W) nanosheets by embedding MeS_x for hydrogen evolution reaction. *Electrochim. Acta* **2018**, *292*, 136–141. [CrossRef]
15. Hasani, A.; Nguyen, T.P.; Tekalgne, M.; Van Le, Q.; Choi, K.S.; Lee, T.H.; Jung Park, T.; Jang, H.W.; Kim, S.Y. The role of metal dopants in WS_2 nanoflowers in enhancing the hydrogen evolution reaction. *Appl. Catal. A* **2018**, *567*, 73–79. [CrossRef]

16. Do, H.H.; Nguyen, D.L.T.; Nguyen, X.C.; Le, T.-H.; Nguyen, T.P.; Trinh, Q.T.; Ahn, S.H.; Vo, D.-V.N.; Kim, S.Y.; Le, Q.V. Recent progress in TiO_2-based photocatalysts for hydrogen evolution reaction: A review. *Arab. J. Chem.* **2020**, *13*, 3653–3671. [CrossRef]
17. Qin, Y.; Li, H.; Lu, J.; Meng, F.; Ma, C.; Yan, Y.; Meng, M. Nitrogen-doped hydrogenated TiO_2 modified with CdS nanorods with enhanced optical absorption, charge separation and photocatalytic hydrogen evolution. *Chem. Eng. J.* **2020**, *384*, 123275. [CrossRef]
18. Shi, W.; Li, M.; Huang, X.; Ren, H.; Yan, C.; Guo, F. Facile synthesis of 2D/2D $Co_3(PO_4)_2$/g-C_3N_4 heterojunction for highly photocatalytic overall water splitting under visible light. *Chem. Eng. J.* **2020**, *382*, 122960. [CrossRef]
19. Mishra, A.; Mehta, A.; Basu, S.; Shetti, N.P.; Reddy, K.R.; Aminabhavi, T.M. Graphitic carbon nitride (g–C_3N_4)-based metal-free photocatalysts for water splitting: A review. *Carbon* **2019**, *149*, 693–721. [CrossRef]
20. Fang, X.; Gao, R.; Yang, Y.; Yan, D. A Cocrystal Precursor Strategy for Carbon-Rich Graphitic Carbon Nitride toward High-Efficiency Photocatalytic Overall Water Splitting. *iScience* **2019**, *16*, 22–30. [CrossRef]
21. Ehrmaier, J.; Karsili, T.N.V.; Sobolewski, A.L.; Domcke, W. Mechanism of Photocatalytic Water Splitting with Graphitic Carbon Nitride: Photochemistry of the Heptazine-Water Complex. *J. Phys. Chem. A* **2017**, *121*, 4754–4764. [CrossRef]
22. Srinivasu, K.; Ghosh, S.K. Photocatalytic splitting of water on s-triazine based graphitic carbon nitride: An ab initio investigation. *J. Mater. Chem. A* **2015**, *3*, 23011–23016. [CrossRef]
23. Pan, Z.; Pan, N.; Chen, L.; He, J.; Zhang, M. Flower-like MOF-derived Co–N-doped carbon composite with remarkable activity and durability for electrochemical hydrogen evolution reaction. *Int. J. Hydrog. Energy* **2019**, *44*, 30075–30083. [CrossRef]
24. Duan, J.; Chen, S.; Zhao, C. Ultrathin metal-organic framework array for efficient electrocatalytic water splitting. *Nat. Commun.* **2017**, *8*, 15341. [CrossRef] [PubMed]
25. Chen, W.; Pei, J.; He, C.-T.; Wan, J.; Ren, H.; Wang, Y.; Dong, J.; Wu, K.; Cheong, W.-C.; Mao, J.; et al. Single Tungsten Atoms Supported on MOF-Derived N-Doped Carbon for Robust Electrochemical Hydrogen Evolution. *Adv. Mater.* **2018**, *30*, 1800396. [CrossRef] [PubMed]
26. Li, Y.; Peng, Y.-K.; Hu, L.; Zheng, J.; Prabhakaran, D.; Wu, S.; Puchtler, T.J.; Li, M.; Wong, K.-Y.; Taylor, R.A.; et al. Photocatalytic water splitting by N-TiO_2 on MgO (111) with exceptional quantum efficiencies at elevated temperatures. *Nat. Commun.* **2019**, *10*, 4421. [CrossRef]
27. Wang, Y.; Zhang, J. Structural engineering of transition metal-based nanostructured electrocatalysts for efficient water splitting. *Front. Chem. Sci. Eng.* **2018**, *12*, 838–854. [CrossRef]
28. Cheng, Y.-W.; Dai, J.-H.; Zhang, Y.-M.; Song, Y. Two-Dimensional, Ordered, Double Transition Metal Carbides (MXenes): A New Family of Promising Catalysts for the Hydrogen Evolution Reaction. *J. Phys. Chem. C* **2018**, *122*, 28113–28122. [CrossRef]
29. Esposito, D.V.; Hunt, S.T.; Kimmel, Y.C.; Chen, J.G. A New Class of Electrocatalysts for Hydrogen Production from Water Electrolysis: Metal Monolayers Supported on Low-Cost Transition Metal Carbides. *J. Am. Chem. Soc.* **2012**, *134*, 3025–3033. [CrossRef]
30. Miao, M.; Pan, J.; He, T.; Yan, Y.; Xia, B.Y.; Wang, X. Molybdenum Carbide-Based Electrocatalysts for Hydrogen Evolution Reaction. *Chem. Eur.* **2017**, *23*, 10947–10961. [CrossRef]
31. Naguib, M.; Mochalin, V.N.; Barsoum, M.W.; Gogotsi, Y. 25th Anniversary Article: MXenes: A New Family of Two-Dimensional Materials. *Adv. Mater.* **2014**, *26*, 992–1005. [CrossRef]
32. Naguib, M.; Mashtalir, O.; Carle, J.; Presser, V.; Lu, J.; Hultman, L.; Gogotsi, Y.; Barsoum, M.W. Two-Dimensional Transition Metal Carbides. *ACS Nano* **2012**, *6*, 1322–1331. [CrossRef] [PubMed]
33. Barsoum, M.W. The $M_{N+1}AX_N$ phases: A new class of solids: Thermodynamically stable nanolaminates. *Prog. Solid State Chem.* **2000**, *28*, 201–281. [CrossRef]
34. Jun, B.-M.; Kim, S.; Heo, J.; Park, C.M.; Her, N.; Jang, M.; Huang, Y.; Han, J.; Yoon, Y. Review of MXenes as new nanomaterials for energy storage/delivery and selected environmental applications. *Nano Res.* **2019**, *12*, 471–487. [CrossRef]
35. Verger, L.; Natu, V.; Carey, M.; Barsoum, M.W. MXenes: An Introduction of Their Synthesis, Select Properties, and Applications. *Trends Chem.* **2019**, *1*, 656–669. [CrossRef]
36. Anasori, B.; Lukatskaya, M.R.; Gogotsi, Y. 2D metal carbides and nitrides (MXenes) for energy storage. *Nat. Rev. Mater.* **2017**, *2*, 16098. [CrossRef]

37. Pang, J.; Mendes, R.G.; Bachmatiuk, A.; Zhao, L.; Ta, H.Q.; Gemming, T.; Liu, H.; Liu, Z.; Rummeli, M.H. Applications of 2D MXenes in energy conversion and storage systems. *Chem. Soc. Rev.* **2019**, *48*, 72–133. [CrossRef]
38. Alhabeb, M.; Maleski, K.; Anasori, B.; Lelyukh, P.; Clark, L.; Sin, S.; Gogotsi, Y. Guidelines for Synthesis and Processing of Two-Dimensional Titanium Carbide ($Ti_3C_2T_x$ MXene). *Chem. Mater.* **2017**, *29*, 7633–7644. [CrossRef]
39. Eklund, P.; Beckers, M.; Jansson, U.; Högberg, H.; Hultman, L. The $M_{n+1}AX_n$ phases: Materials science and thin-film processing. *Thin Solid Films* **2010**, *518*, 1851–1878. [CrossRef]
40. Anasori, B.; Gogotsi, Y. Introduction to 2D Transition Metal Carbides and Nitrides (MXenes). In *2D Metal Carbides and Nitrides (MXenes): Structure, Properties and Applications*; Anasori, B., Gogotsi, Y., Eds.; Springer International Publishing: Cham, Switzerland, 2019; pp. 3–12. [CrossRef]
41. Zhan, X.; Si, C.; Zhou, J.; Sun, Z. MXene and MXene-based composites: synthesis, properties and environment-related applications. *Nanoscale Horiz.* **2020**, *5*, 235–258. [CrossRef]
42. Jiang, X.; Kuklin, A.V.; Baev, A.; Ge, Y.; Ågren, H.; Zhang, H.; Prasad, P.N. Two-dimensional MXenes: From morphological to optical, electric, and magnetic properties and applications. *Phys. Rep.* **2020**, *848*, 1–58. [CrossRef]
43. Cheng, L.; Li, X.; Zhang, H.; Xiang, Q. Two-Dimensional Transition Metal MXene-Based Photocatalysts for Solar Fuel Generation. *J. Phys. Chem. Lett.* **2019**, *10*, 3488–3494. [CrossRef] [PubMed]
44. Ye, M.; Wang, X.; Liu, E.; Ye, J.; Wang, D. Boosting the Photocatalytic Activity of P25 for Carbon Dioxide Reduction by using a Surface-Alkalinized Titanium Carbide MXene as Cocatalyst. *ChemSusChem* **2018**, *11*, 1606–1611. [CrossRef] [PubMed]
45. An, X.; Wang, W.; Wang, J.; Duan, H.; Shi, J.; Yu, X. The synergetic effects of Ti_3C_2 MXene and Pt as co-catalysts for highly efficient photocatalytic hydrogen evolution over g-C_3N_4. *Phys. Chem. Chem. Phys.* **2018**, *20*, 11405–11411. [CrossRef] [PubMed]
46. Li, Y.; Ding, L.; Liang, Z.; Xue, Y.; Cui, H.; Tian, J. Synergetic effect of defects rich MoS_2 and Ti_3C_2 MXene as cocatalysts for enhanced photocatalytic H_2 production activity of TiO_2. *Chem. Eng. J.* **2020**, *383*, 123178. [CrossRef]
47. Zhang, C.; Anasori, B.; Seral-Ascaso, A.; Park, S.-H.; McEvoy, N.; Shmeliov, A.; Duesberg, G.S.; Coleman, J.N.; Gogotsi, Y.; Nicolosi, V. Transparent, Flexible, and Conductive 2D Titanium Carbide (MXene) Films with High Volumetric Capacitance. *Adv. Mater.* **2017**, *29*, 1702678. [CrossRef]
48. Gao, G.; O'Mullane, A.P.; Du, A. 2D MXenes: A New Family of Promising Catalysts for the Hydrogen Evolution Reaction. *ACS Catal.* **2017**, *7*, 494–500. [CrossRef]
49. Zhu, J.; Ha, E.; Zhao, G.; Zhou, Y.; Huang, D.; Yue, G.; Hu, L.; Sun, N.; Wang, Y.; Lee, L.Y.S.; et al. Recent advance in MXenes: A promising 2D material for catalysis, sensor and chemical adsorption. *Coord. Chem. Rev.* **2017**, *352*, 306–327. [CrossRef]
50. Nguyen, T.P.; Tuan Nguyen, D.M.; Tran, D.L.; Le, H.K.; Vo, D.-V.N.; Lam, S.S.; Varma, R.S.; Shokouhimehr, M.; Nguyen, C.C.; Le, Q.V. MXenes: Applications in electrocatalytic, photocatalytic hydrogen evolution reaction and CO_2 reduction. *Mol. Catal.* **2020**, *486*, 110850. [CrossRef]
51. Jiang, Q.; Lei, Y.; Liang, H.; Xi, K.; Xia, C.; Alshareef, H.N. Review of MXene electrochemical microsupercapacitors. *Energy Storage Mater.* **2020**, *27*, 78–95. [CrossRef]
52. Su, T.; Hood, Z.D.; Naguib, M.; Bai, L.; Luo, S.; Rouleau, C.M.; Ivanov, I.N.; Ji, H.; Qin, Z.; Wu, Z. Monolayer Ti3C2Tx as an Effective Co-catalyst for Enhanced Photocatalytic Hydrogen Production over TiO_2. *ACS Appl. Energy Mater.* **2019**, *2*, 4640–4651. [CrossRef]
53. Zhang, J.; Zhao, Y.; Guo, X.; Chen, C.; Dong, C.-L.; Liu, R.-S.; Han, C.-P.; Li, Y.; Gogotsi, Y.; Wang, G. Single platinum atoms immobilized on an MXene as an efficient catalyst for the hydrogen evolution reaction. *Nat. Catal.* **2018**, *1*, 985–992. [CrossRef]
54. Yuan, W.; Cheng, L.; An, Y.; Wu, H.; Yao, N.; Fan, X.; Guo, X. MXene Nanofibers as Highly Active Catalysts for Hydrogen Evolution Reaction. *ACS Sustain. Chem. Eng.* **2018**, *6*, 8976–8982. [CrossRef]
55. Li, Y.; Ding, L.; Guo, Y.; Liang, Z.; Cui, H.; Tian, J. Boosting the Photocatalytic Ability of g-C_3N_4 for Hydrogen Production by Ti_3C_2 MXene Quantum Dots. *ACS Appl. Mater. Interfaces* **2019**, *11*, 41440–41447. [CrossRef] [PubMed]

56. Sun, Y.; Jin, D.; Sun, Y.; Meng, X.; Gao, Y.; Dall'Agnese, Y.; Chen, G.; Wang, X.-F. g-C_3N_4/$Ti_3C_2T_x$ (MXenes) composite with oxidized surface groups for efficient photocatalytic hydrogen evolution. *J. Mater. Chem. A* **2018**, *6*, 9124–9131. [CrossRef]
57. Zhang, X.; Ma, Z.; Zhao, X.; Tang, Q.; Zhou, Z. Computational studies on structural and electronic properties of functionalized MXene monolayers and nanotubes. *J. Mater. Chem. A* **2015**, *3*, 4960–4966. [CrossRef]
58. Xie, Y.; Kent, P.R.C. Hybrid density functional study of structural and electronic properties of functionalized $Ti_{n+1}X_n$ (X = C, N) monolayers. *Phys. Rev. B* **2013**, *87*, 235441. [CrossRef]
59. Berdiyorov, G.R. Effect of surface functionalization on the electronic transport properties of Ti_3C_2 MXene. *EPL (Europhys. Lett.)* **2015**, *111*, 67002. [CrossRef]
60. Berdiyorov, G.R. Optical properties of functionalized $Ti_3C_2T_2$ (T = F, O, OH) MXene: First-principles calculations. *AIP Advances* **2016**, *6*, 055105. [CrossRef]
61. Ran, J.; Gao, G.; Li, F.-T.; Ma, T.-Y.; Du, A.; Qiao, S.-Z. Ti_3C_2 MXene co-catalyst on metal sulfide photo-absorbers for enhanced visible-light photocatalytic hydrogen production. *Nat. Commun.* **2017**, *8*, 13907. [CrossRef]
62. Yang, Y.; Zhang, D.; Xiang, Q. Plasma-modified $Ti_3C_2T_x$/CdS hybrids with oxygen-containing groups for high-efficiency photocatalytic hydrogen production. *Nanoscale* **2019**, *11*, 18797–18805. [CrossRef]
63. Xu, F.; Zhang, D.; Liao, Y.; Wang, G.; Shi, X.; Zhang, H.; Xiang, Q. Synthesis and photocatalytic H_2-production activity of plasma-treated $Ti_3C_2T_x$ MXene modified graphitic carbon nitride. *J. Am. Ceram. Soc.* **2020**, *103*, 849–858. [CrossRef]
64. Miyoshi, A.; Nishioka, S.; Maeda, K. Water Splitting on Rutile TiO_2-Based Photocatalysts. *Chem. Eur.* **2018**, *24*, 18204–18219. [CrossRef] [PubMed]
65. Ni, M.; Leung, M.K.H.; Leung, D.Y.C.; Sumathy, K. A review and recent developments in photocatalytic water-splitting using TiO_2 for hydrogen production. *Renew. Sustain. Energy Rev.* **2007**, *11*, 401–425. [CrossRef]
66. Li, R.; Weng, Y.; Zhou, X.; Wang, X.; Mi, Y.; Chong, R.; Han, H.; Li, C. Achieving overall water splitting using titanium dioxide-based photocatalysts of different phases. *Energy Environ. Sci.* **2015**, *8*, 2377–2382. [CrossRef]
67. Zhuang, Y.; Liu, Y.; Meng, X. Fabrication of TiO_2 nanofibers/MXene Ti_3C_2 nanocomposites for photocatalytic H_2 evolution by electrostatic self-assembly. *Appl. Surf. Sci.* **2019**, *496*, 143647. [CrossRef]
68. Liu, X.; Chen, C. Mxene enhanced the photocatalytic activity of ZnO nanorods under visible light. *Mater. Lett.* **2020**, *261*, 127127. [CrossRef]
69. Tso, S.; Li, W.-S.; Wu, B.-H.; Chen, L.-J. Enhanced H_2 production in water splitting with CdS-ZnO core-shell nanowires. *Nano Energy* **2018**, *43*, 270–277. [CrossRef]
70. Garg, P.; Bhauriyal, P.; Mahata, A.; Rawat, K.S.; Pathak, B. Role of Dimensionality for Photocatalytic Water Splitting: CdS Nanotube versus Bulk Structure. *Chemphyschem* **2019**, *20*, 383–391. [CrossRef]
71. Chen, X.; Shangguan, W. Hydrogen production from water splitting on CdS-based photocatalysts using solar light. *Front. Energy* **2013**, *7*, 111–118. [CrossRef]
72. Wang, Z.; Wang, J.; Li, L.; Zheng, J.; Jia, S.; Chen, J.; Liu, B.; Zhu, Z. Fabricating efficient CdSe–CdS photocatalyst systems by spatially resetting water splitting sites. *J. Mater. Chem. A* **2017**, *5*, 20131–20135. [CrossRef]
73. Li, M.; Cui, Z.; Li, E. Silver-modified MoS_2 nanosheets as a high-efficiency visible-light photocatalyst for water splitting. *Ceram. Int.* **2019**, *45*, 14449–14456. [CrossRef]
74. Lin, L.; Huang, S.; Zhu, Y.; Du, B.; Zhang, Z.; Chen, C.; Wang, X.; Zhang, N. Construction of CdS/MoS_2 heterojunction from core–shell MoS_2@Cd-MOF for efficient photocatalytic hydrogen evolution. *Dalton Trans.* **2019**, *48*, 2715–2721. [CrossRef] [PubMed]
75. Han, B.; Hu, Y.H. MoS_2 as a co-catalyst for photocatalytic hydrogen production from water. *Energy Sci. Eng.* **2016**, *4*, 285–304. [CrossRef]
76. Xiang, Q.; Cheng, F.; Lang, D. Hierarchical Layered WS_2/Graphene-Modified CdS Nanorods for Efficient Photocatalytic Hydrogen Evolution. *ChemSusChem* **2016**, *9*, 996–1002. [CrossRef]
77. Kumar, R.; Das, D.; Singh, A.K. C_2N/WS_2 van der Waals type-II heterostructure as a promising water splitting photocatalyst. *J. Catal.* **2018**, *359*, 143–150. [CrossRef]
78. Reddy, D.A.; Park, H.; Ma, R.; Kumar, D.P.; Lim, M.; Kim, T.K. Heterostructured WS_2-MoS_2 Ultrathin Nanosheets Integrated on CdS Nanorods to Promote Charge Separation and Migration and Improve Solar-Driven Photocatalytic Hydrogen Evolution. *ChemSusChem* **2017**, *10*, 1563–1570. [CrossRef]

79. Xiao, R.; Zhao, C.; Zou, Z.; Chen, Z.; Tian, L.; Xu, H.; Tang, H.; Liu, Q.; Lin, Z.; Yang, X. In situ fabrication of 1D CdS nanorod/2D Ti_3C_2 MXene nanosheet Schottky heterojunction toward enhanced photocatalytic hydrogen evolution. *Appl. Catal. B* **2019**, *268*, 118382. [CrossRef]
80. Tie, L.; Yang, S.; Yu, C.; Chen, H.; Liu, Y.; Dong, S.; Sun, J.; Sun, J. In situ decoration of ZnS nanoparticles with Ti_3C_2 MXene nanosheets for efficient photocatalytic hydrogen evolution. *J. Colloid Interface Sci.* **2019**, *545*, 63–70. [CrossRef]
81. Cheng, L.; Chen, Q.; Li, J.; Liu, H. Boosting the photocatalytic activity of $CdLa_2S_4$ for hydrogen production using Ti_3C_2 MXene as a co-catalyst. *Appl. Catal. B* **2019**, *267*, 118379. [CrossRef]
82. Tian, P.; He, X.; Zhao, L.; Li, W.; Fang, W.; Chen, H.; Zhang, F.; Huang, Z.; Wang, H. Ti_3C_2 nanosheets modified Zr-MOFs with Schottky junction for boosting photocatalytic HER performance. *Sol. Energy* **2019**, *188*, 750–759. [CrossRef]
83. Dong, J.; Shi, Y.; Huang, C.; Wu, Q.; Zeng, T.; Yao, W. A New and stable Mo-Mo_2C modified g-C_3N_4 photocatalyst for efficient visible light photocatalytic H_2 production. *Appl. Catal. B* **2019**, *243*, 27–35. [CrossRef]
84. Wen, J.; Xie, J.; Chen, X.; Li, X. A review on g-C_3N_4-based photocatalysts. *Appl. Surf. Sci.* **2017**, *391*, 72–123. [CrossRef]
85. Zou, Y.; Ma, D.; Sun, D.; Mao, S.; He, C.; Wang, Z.; Ji, X.; Shi, J.-W. Carbon nanosheet facilitated charge separation and transfer between molybdenum carbide and graphitic carbon nitride toward efficient photocatalytic H_2 production. *Appl. Surf. Sci.* **2019**, *473*, 91–101. [CrossRef]
86. Su, T.; Hood, Z.D.; Naguib, M.; Bai, L.; Luo, S.; Rouleau, C.M.; Ivanov, I.N.; Ji, H.; Qin, Z.; Wu, Z. 2D/2D heterojunction of Ti_3C_2/g-C_3N_4 nanosheets for enhanced photocatalytic hydrogen evolution. *Nanoscale* **2019**, *11*, 8138–8149. [CrossRef] [PubMed]
87. Lin, P.; Shen, J.; Yu, X.; Liu, Q.; Li, D.; Tang, H. Construction of Ti_3C_2 MXene/O-doped g-C_3N_4 2D-2D Schottky-junction for enhanced photocatalytic hydrogen evolution. *Ceram. Int.* **2019**, *45*, 24656–24663. [CrossRef]
88. Tian, P.; He, X.; Zhao, L.; Li, W.; Fang, W.; Chen, H.; Zhang, F.; Huang, Z.; Wang, H. Enhanced charge transfer for efficient photocatalytic H_2 evolution over UiO-66-NH_2 with annealed $Ti_3C_2T_x$ MXenes. *Int. J. Hydrog. Energy* **2019**, *44*, 788–800. [CrossRef]
89. Peng, C.; Wei, P.; Li, X.; Liu, Y.; Cao, Y.; Wang, H.; Yu, H.; Peng, F.; Zhang, L.; Zhang, B.; et al. High efficiency photocatalytic hydrogen production over ternary Cu/TiO_2@$Ti_3C_2T_x$ enabled by low-work-function 2D titanium carbide. *Nano Energy* **2018**, *53*, 97–107. [CrossRef]
90. Li, Y.; Yang, S.; Liang, Z.; Xue, Y.; Cui, H.; Tian, J. 1T-MoS_2 nanopatch/Ti_3C_2 MXene/TiO_2 nanosheet hybrids for efficient photocatalytic hydrogen evolution. *Mater. Chem. Front.* **2019**, *3*, 2673–2680. [CrossRef]
91. Li, Y.; Ding, L.; Yin, S.; Liang, Z.; Xue, Y.; Wang, X.; Cui, H.; Tian, J. Photocatalytic H_2 Evolution on TiO_2 Assembled with Ti_3C_2 MXene and Metallic 1T-WS_2 as Co-catalysts. *Nano-Micro Lett.* **2019**, *12*, 6. [CrossRef]
92. Yu, M.; Wang, Z.; Liu, J.; Sun, F.; Yang, P.; Qiu, J. A hierarchically porous and hydrophilic 3D nickel–iron/MXene electrode for accelerating oxygen and hydrogen evolution at high current densities. *Nano Energy* **2019**, *63*, 103880. [CrossRef]
93. Zhang, M.; Qin, J.; Rajendran, S.; Zhang, X.; Liu, R. Heterostructured d-Ti_3C_2/TiO_2/g-C_3N_4 Nanocomposites with Enhanced Visible-Light Photocatalytic Hydrogen Production Activity. *ChemSusChem* **2018**, *11*, 4226–4236. [CrossRef] [PubMed]
94. Ramalingam, V.; Varadhan, P.; Fu, H.-C.; Kim, H.; Zhang, D.; Chen, S.; Song, L.; Ma, D.; Wang, Y.; Alshareef, H.N.; et al. Heteroatom-Mediated Interactions between Ruthenium Single Atoms and an MXene Support for Efficient Hydrogen Evolution. *Adv. Mater.* **2019**, *31*, 1903841. [CrossRef] [PubMed]
95. Li, Y.; Yin, Z.; Ji, G.; Liang, Z.; Xue, Y.; Guo, Y.; Tian, J.; Wang, X.; Cui, H. 2D/2D/2D heterojunction of Ti_3C_2 MXene/MoS_2 nanosheets/TiO_2 nanosheets with exposed (001) facets toward enhanced photocatalytic hydrogen production activity. *Appl. Catal. B* **2019**, *246*, 12–20. [CrossRef]
96. Su, T.; Peng, R.; Hood, Z.D.; Naguib, M.; Ivanov, I.N.; Keum, J.K.; Qin, Z.; Guo, Z.; Wu, Z. One-Step Synthesis of Nb_2O_5/C/Nb_2C (MXene) Composites and Their Use as Photocatalysts for Hydrogen Evolution. *ChemSusChem* **2018**, *11*, 688–699. [CrossRef]

97. Pan, L.; Mei, H.; Liu, H.; Pan, H.; Zhao, X.; Jin, Z.; Zhu, G. High-efficiency carrier separation heterostructure improve the photocatalytic hydrogen production of sulfide. *J. Alloys Compd.* **2020**, *817*, 153242. [CrossRef]
98. Sun, Y.; Sun, Y.; Meng, X.; Gao, Y.; Dall'Agnese, Y.; Chen, G.; Dall'Agnese, C.; Wang, X.-F. Eosin Y-sensitized partially oxidized Ti_3C_2 MXene for photocatalytic hydrogen evolution. *Catal. Sci. Technol.* **2019**, *9*, 310–315. [CrossRef]